Journal of Quantitative Spectroscopy & Radiative Transfer 188 (2017) 142–147

Contents lists available at ScienceDirect

Journal of Quantitative Spectroscopy & Radiative Transfer

journal homepage: www.elsevier.com/locate/jqsrt

Identification of precipitation onset based on Cloudsat observations

Yu Wang [a,*], Yujue Chen [a], Yunfei Fu [a], Guosheng Liu [b]

[a] School of Earth and Space Sciences, University of Science and Technology of China, Hefei, Anhui 230026, PR China
[b] Department of Earth, Ocean and Atmospheric Science, Florida State University, Tallahassee, FL, USA

ARTICLE INFO

Article history:
Received 20 October 2015
Received in revised form
15 June 2016
Accepted 17 June 2016
Available online 22 June 2016

Keywords:
Identification of precipitation onset
Cloud profiling radar
Radar reflectivity threshold
Liquid water path threshold

ABSTRACT

Observations of cloud vertical structure by Cloud Profiling Radar on CloudSat satellite provide a unique opportunity to globally identify the onset of precipitation. In this study, based on a conceptual model for an adiabatic cloud, a new method to determine the onset of precipitation in marine warm clouds is developed. The new method uses the slope of radar reflectivities near the cloud top, which gradually reverses its signs as drizzle occurs. By analyzing multiyear CloudSat data, it is found that globally the radar reflectivity threshold for precipitation onset varies from −18 to −13 dBZ with an average value of −16 dBZ. The corresponding liquid water path threshold for precipitation onset is also studied by analyzing satellite microwave observations collocated with CloudSat data. Results show that the liquid water path threshold is 190 g m^{-2} as a global mean, varying from 150 to over 300 g m^{-2} depending on regions.

1. Introduction

Determining the onset of precipitation is important to parameterize precipitation processes in numerical models, to develop remote sensing retrieval algorithms, and to understand aerosol indirect effect. In most numerical weather and climate prediction models, the conversion from cloud water to rain water is usually represented by bulk parameterization schemes such as autoconversion scheme for warm clouds [1]. Precipitation produced by models is very sensitive to whether to select mixing ratio or cloud droplet radius as threshold for precipitation onset [2], and incorrect onset threshold could lead to untimely formation of rain, and wrong partitioning between cloud and rain water amounts in models [3,4]. For passive microwave remote sensing, the identification of the onset of precipitation is the first step to distinguish between cloud liquid water and rainfall before retrieving them by emission-based algorithms [5]. Moreover, drizzles as the indicator of precipitation onset, make an important impact on cloud water content retrieval for cloud radar observations [6,7]. Additionally, the second indirect effect of aerosols postulates that anthropogenic aerosols may affect the onset of precipitation [8].

It is known that the onset of precipitation is related to cloud water amount and cloud droplet size [9,10]. Therefore, determining the onset of precipitation by a threshold of liquid water path or effective radius is widely used. However, there are large discrepancies as to what value to use as the precipitation threshold among different investigators [11]. For liquid water path, a threshold of 180 g m^{-2} is chosen in the unified microwave ocean retrieval algorithm of Wentz [12] and Wentz and Spencer [13], while much larger values (300 g m^{-2} or even 500 g m^{-2}) are used in other precipitation retrieval algorithms [14–16]. With respect to cloud droplet size, the

* Corresponding author.
E-mail address: wangyu09@ustc.edu.cn (Y. Wang).

http://dx.doi.org/10.1016/j.jqsrt.2016.06.028

threshold of effective radius of 15 μm or larger has been used [17–20]. Precipitation formation is a complex process governed by cloud dynamics and thermodynamics [21,22]. One reason why the above uncertainties in threshold values exist arises from the lack of direct global observations for precipitation onset [23].

CloudSat, the first satellite carrying a 94 GHz Cloud Profiling Radar (CPR), provides the opportunity for us to identify the onset of precipitation on global scale. Based on CPR and other ground-based cloud radar observations, the threshold of radar reflectivity discriminating between precipitating and nonprecipitating clouds has been proposed and discussed by several investigators. Matrosov et al. [7] and Kawamoto and Suzuki [24] used radar reflectivity of −15 dBZ to eliminate the influence of drizzle on the relationship between radar reflectivity and cloud liquid water content. This threshold was also used by several other investigators for identifying precipitating clouds [25–28]. Kogan et al. [29] chose −17 dBZ as precipitation threshold and found that this value is well correlated with the presence of droplets greater than 25 μm in radius. A lower value of threshold of −20 dBZ was adopted in Mace and Sassen [30] and Kato et al. [31]. Wang and Geerts [32] suggested that the threshold of radar reflectivity in the cloud layer would vary from −19 to −16 dBZ depending on height. For such a wide range of threshold values, Liu et al. [33] theoretically explained it as a function of the cloud droplet concentration.

In this study, a new method to determine the onset of warm cloud precipitation is developed based on CPR reflectivity vertical profile. The global distribution of the threshold and its possible dependence on cloud structure are also explored. Additionally, the liquid water path corresponding to the onset of precipitation is studied.

2. Data and method

In this study, the standard CloudSat radar reflectivity product [34] is used, which contains radar reflectivity values at a 1.7 km (along track) × 1.4 km (across track) horizontal resolution and 240 m in vertical resolution in 150 vertical bins. Data of the lowest 4 bins (~1 km deep) are excluded for the data analysis to avoid possible contamination by surface. Cloud temperature is determined by European Center for Medium-Range Weather Forecasts (ECMWF) objective analysis, which has been collocated with CloudSat data [35]. Our study focuses on warm cloud only. Therefore, only those radar reflectivity profiles with cloud top temperature higher than 273 K are analyzed. To estimate cloud liquid water path, brightness temperatures from Advanced Microwave Scanning Radiometer for Earth Observing System (AMSR-E) on Aqua satellite are also used. Aqua and CloudSat are both on the A-Train constellation; AMSR-E and CPR observations can be considered simultaneous. Liquid water path is retrieved based on the method of Wang et al. [36].

In an idealized non-precipitating adiabatic warm cloud, the liquid water content (LWC) increases linearly upward from cloud base [37]. Though the observed LWC in actual clouds is often about 50–80% of the adiabatic value due to mixing between the rising air in clouds and dry environmental air, observations have shown that LWC in nonprecipitating clouds generally increases linearly with height and the maximum LWC presents near the cloud top [38,39]. Moreover, because the drop number concentration within a nonprecipitating cloud is generally constant with respect to height, the mean cloud drop size increases with height [37]. As a result, for nonprecipitating warm clouds, radar reflectivity should increase with height. As the cloud develops, some of the water drops grow to a radius between 15 and 25 μm [40–44], a critical size for coalescence to take place, and then drizzles start to occur. Note that at the time when drizzle drops begin to form, the initial source of drizzles is generally near the cloud top where there exist the largest cloud drops and the highest LWC. The above features have been revealed by both observations and model simulations [6,45]. After drizzle drops form, they fall downward in the clouds as they further grow by accretion of small cloud particles [46]. Considering that the radar reflectivity factor is proportional to the sixth moment of the drop size distribution, the radar reflectivity would increase from cloud top downward after drizzle drops form and then fall.

In summary, radar reflectivity would increase upward near cloud top in warm nonprecipitating clouds, but would decrease when drizzle starts, which has also been suggested by Wang and Geerts [32] and Leon et al. [23]. Our precipitation onset detection algorithm will apply the above logic to CloudSat observations. As discussed above, drizzle drops initially occur near the cloud top. Ideally, we would like to use CPR returns at the highest bins for the drizzle detection algorithm. However, the highest bin in radar reflectivity profile is often not fully filled by cloud body, which makes it hard to compare with the reflectivity values in the bins below. Therefore, in this study we use the second and third bins from cloud top to calculate the radar reflectivity vertical variation and then judge whether the cloud is precipitating. That is, if the radar reflectivity in the second bin (counted from top down) is larger than that in the third bin, the cloud is classified as nonprecipitating, otherwise precipitating. The transition between the two indicates the onset of precipitation. For shallow clouds, evaporation of drizzle drops after falling out of clouds could complicate the interpretation of reflectivity profiles. To minimize this problem, only those profiles with reflectivity value at the 4th bin (from cloud top) higher than −25 dBZ are included in the analysis.

To illustrate how the precipitation identification method works, we show next the variation of radar reflectivity profiles with its maximum value in the top 2nd and 3rd bins (called MaxR hereafter) for the following two subtropical coastal regions with prevailing low-level marine clouds: Californian (15–30°N, 120–130°W) and Peruvian (10–30°S, 70–90°W) coasts, in June, July and August of 2006 through 2009. As shown in Fig. 1, for both Californian and Peruvian coasts, when MaxR is lower than −15 dBZ, the radar reflectivity in the upper bin is higher than that in the lower bin, which is the typical characteristic of nonprecipitating clouds. Once MaxR is higher than −15 dBZ, the radar reflectivity in the lower bin exceeds that in the higher bin, indicating the presence of drizzles. Moreover, with increasing MaxR, the radar

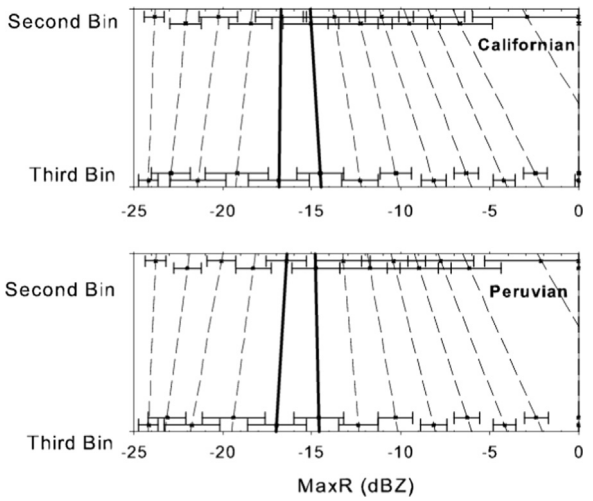

Fig. 1. The variation of reflectivity profiles of the top second and third bins from cloud top as the maximum reflectivity value (MaxR) increases for Californian (top) and Peruvian (bottom) coastal regions. Solid lines indicate the position where the reflectivity profile slope reveres signs, i.e., precipitation onset, and the error bars denote the standard deviations for each profile.

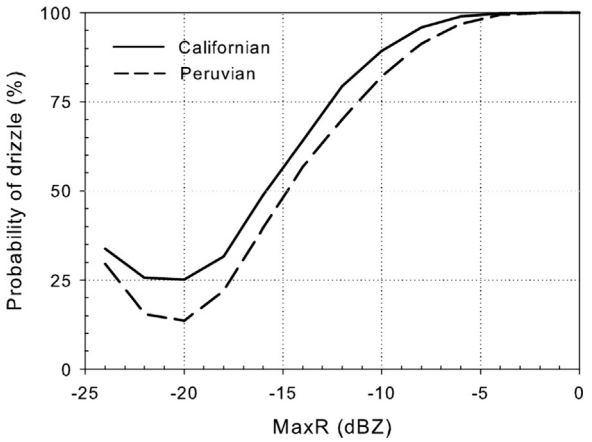

Fig. 2. The probability of drizzle occurrence as a function of MaxR for Californian and Peruvian coastal regions.

reflectivity difference between the two bins gradually increases, implying the increase of drizzles' size with cloud development. The above variation of the radar reflectivity slope with MaxR near the cloud top is consistent with the transformation from nonprecipitating to drizzle clouds. It is noted that the -15 dBZ MaxR found here is similar to the threshold previously used in some of the literatures [7,25,28].

To determine the threshold of precipitation onset as a function of MaxR, the probability of drizzle occurrence in all clouds, based on the relative magnitude of radar reflectivities at the second and third bins as discussed above, is calculated and plotted against MaxR in Fig. 2. It can be seen that the probability increases with MaxR in a similar fashion for the two regions, where 90% (80%) of clouds near the Californian (Peruvian) coasts starts to precipitate when MaxR is -10 dBZ, and almost all clouds are precipitating for MaxR higher than -5 dBZ. Moreover, the 50% probability occurs at MaxR around -15 dBZ, which is in agreement with the result of the value separating between nonprecipitating and precipitating clouds shown in Fig. 1. Therefore, the MaxR value at the 50% probability will be used as the threshold to identify the precipitation onset in this study.

3. Results

3.1. Global distribution of precipitation threshold

To highlight the regional diversity of the precipitation threshold, threshold values of MaxR in every 2.5° (latitude) by 2.5° (longitude) box over the globe are calculated based on CPR observations for four years (2006–2009). The results are shown in Fig. 3. For statistical significance, only those boxes where the sample number around the 50% probability of drizzle occurrence is larger than 1000 are shown. Generally, the threshold over the globe varies from -18 to -13 dBZ. Higher values (> -15 dBZ) are mostly located to the west of land masses where marine boundary layer clouds dominate, i.e., off the Californian, Peruvian, Canarian, Namibian and Australian coasts. The globally averaged MaxR value for precipitation threshold is about -16 dBZ, which is in agreement with the maximum reflectivity threshold of -15 dBZ as widely used in the literature [7].

The variation of MaxR threshold may arise partly from the differences of cloud properties among different cloud types. Thus, mean MaxR threshold as a function of cloud top height and its standard deviation within a $2.5° \times 2.5°$ box are shown in Fig. 4. Clearly, low and horizontally-homogeneous clouds have higher MaxR value of precipitation threshold, and tall and inhomogeneous clouds have lower value of MaxR threshold. This result implies that stratiform clouds seem to have a higher MaxR threshold, while drizzle likely occurs with relatively low MaxR for convective clouds.

Radar reflectivity of a cloud is determined by cloud drop number and drop size. To understand this dependence, radar reflectivity is calculated based on Mie scattering assuming a Gamma size distribution for cloud drops (Fig. 5). In natural clouds, cloud drop concentration generally varies from 2.5×10^7 to 1×10^9 m^{-3} for different air masses depending on the availability of cloud condensation nuclei, the maximum supersaturation in the cloud, size distribution and so on [47,48]. At effective radius of 15 μm, which is often thought to be the precipitation threshold [19], the calculated radar reflectivity in the above cloud drop concentration range varies between -20 and -8 dBZ with a mean value of about -15 dBZ, which is consistent with observations shown in Fig. 4.

3.2. Relation to liquid water path

In many applications, liquid water path (LWP) is used as a threshold for precipitation onset [12,14]. In the following, we attempt to answer such a question: how big LWP is required to start warm cloud precipitation? LWP is retrieved for warm clouds over ocean based on observations of AMSR-E for 4 years (July 2006–June 2010). Here the LWP retrieval is primarily based on brightness

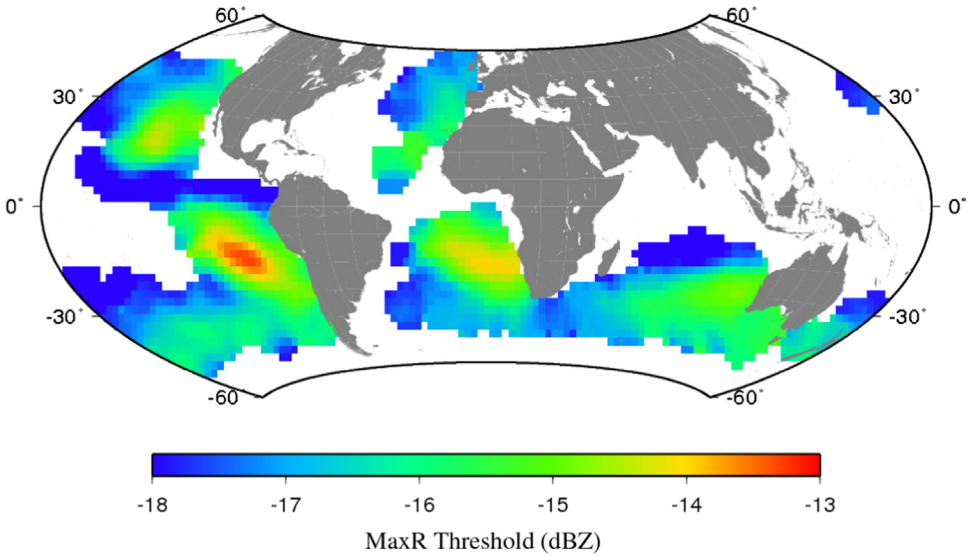

Fig. 3. The global distribution of MaxR values of the precipitation onset threshold.

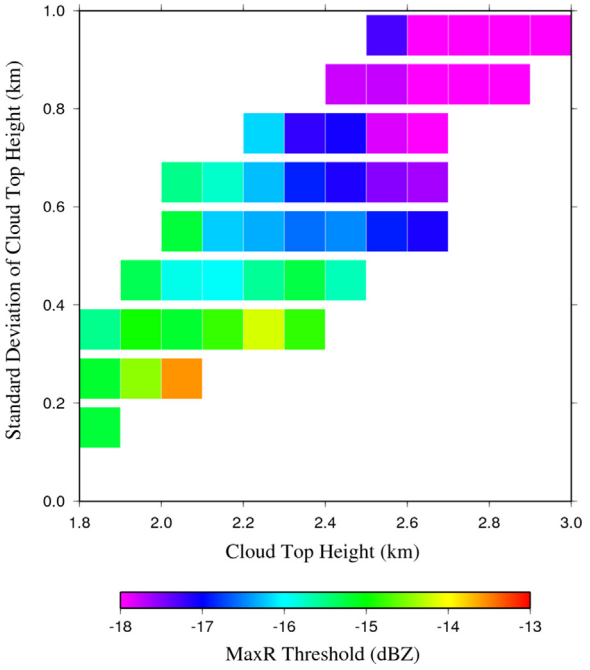

Fig. 4. The variation of mean MaxR threshold as a function of cloud top height and its horizontal variation.

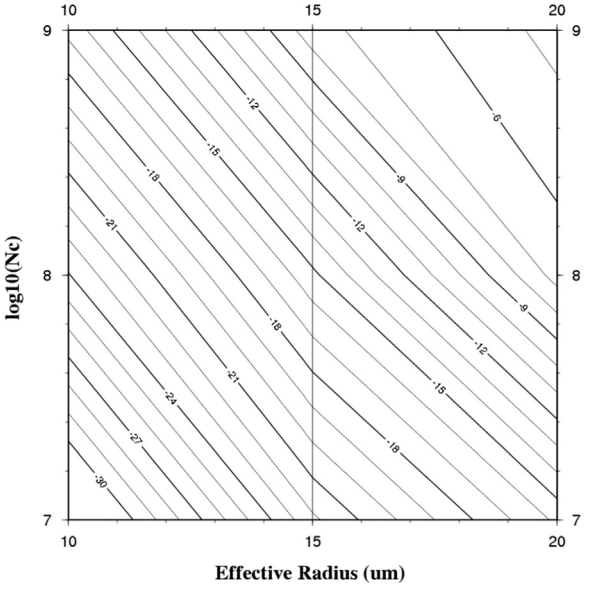

Fig. 5. The variation of simulated CPR reflectivity (dBZ) as a function of cloud drop concentration and effective radius.

temperatures at 37 GHz, and observations at other AMSR-E channels are used to assist in calculating 37 GHz clear-sky brightness temperatures [36]. Collocated CloudSat CPR data are also used in the LWP algorithm for identifying clear-sky scenes. Because of the resolution difference between AMSR-E and CPR, there are generally about 7 samples of CPR in an AMSR-E field-of-view. Therefore, the maximum of MaxR among all CPR samples within an AMSR-E pixel is taken as the MaxR of this pixel.

First, for each 2.5° by 2.5° box over the global ocean, LWP values of those pixels having MaxR lower than the drizzle threshold as defined in the following are selected. From these selected nonprecipitating cloud LWP retrievals in each box, mean value of LWPs between 95% and 98% percentiles is used as the LWP threshold. The reason of not choosing the maximum LWP as threshold is intended to avoid erroneous LWP retrievals when clouds become so close to precipitate. The LWP threshold is then obtained for all available boxes, and shown in Fig. 6. Statistically, the global mean LWP threshold is 190 g m^{-2} with a standard deviation of 35 g m^{-2}, which is comparable to the threshold of 187 g m^{-2} suggested by Chen et al. [49] and 180 g m^{-2} used in Wentz [12]. However, it should be mentioned that this LWP threshold for different regions varies from about

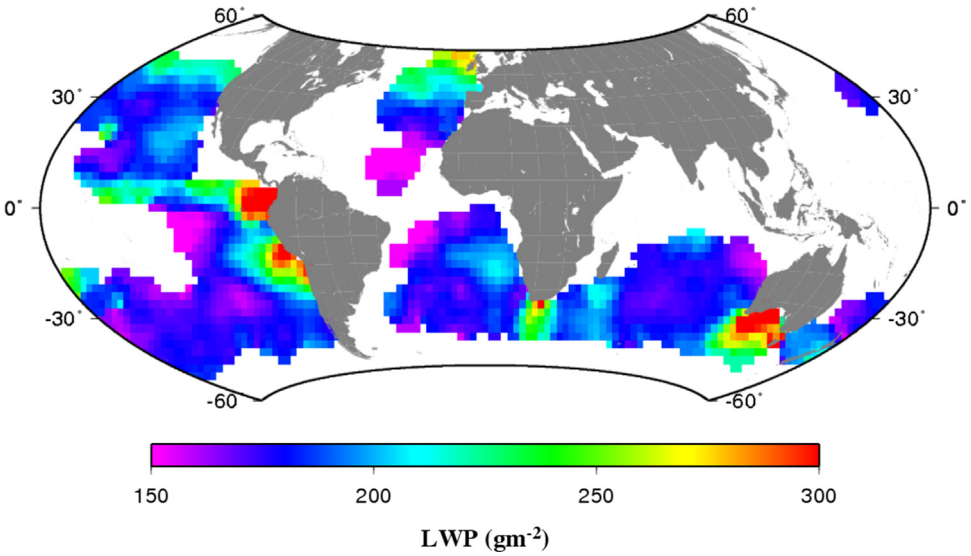

Fig. 6. Similar to Fig. 3, but LWP thresholds for precipitation onset.

150 g m^{-2} in open oceans to more than 300 g m^{-2} near the coasts, which possibly is an evidence of aerosol indirect effect and worth to be further studied in the future.

4. Conclusions

The vertical structure of clouds observed by the CPR on CloudSat satellite offers a unique opportunity to identify the onset of precipitation. In this study, a new method to determine the onset of precipitation for marine warm clouds by CPR reflectivity profiles is presented. In this method, the slope of radar reflectivity in the top portion of clouds is used to identify the presence of drizzles. The method is based on a conceptual model of an adiabatic cloud. Using CPR observations, it is shown that the slope of the radar reflectivities as determined by the top 2nd and 3rd (counted from cloud top) bins in the profiles gradually reverses its signs with radar reflectivity increasing, consistent with the conceptual model of growing cloud drops being transformed to drizzles.

Based on 4 years of CPR measurements, the global distribution of radar reflectivity threshold for precipitation onset is examined. It is found that this threshold varies from −18 to −13 dBZ depending on cloud types. Higher threshold values mostly locate in off-shore stratiform cloud regions, while lower threshold values are in open seas where clouds are more convective. On average, radar reflectivity threshold is about −16 dBZ globally. Using the radar reflectivity threshold, corresponding liquid water path threshold for identifying warm cloud precipitation is also studied. The results show that precipitation is likely to start when liquid water path exceeds 190 g m^{-2} as a global mean, and this threshold varies from about 150 to above 300 g m^{-2} depending on regions.

As discussed in the introduction, the threshold for precipitation onset is required for many applications, and different values have been used so far by investigators. By exploring the utility of CloudSat radar observations, this study takes a fresh view on this problem, and its results, while confirming those of some previous studies, hopefully have put the threshold values on a firmer footing.

Acknowledgments

The authors would like to thank the anonymous reviewers for their valuable comments and suggestions. This study was supported in part by the National Natural Science Foundation of China under Grants 41375030, 91337213 and 41230419. CloudSat data were provided by the NASA CloudSat project and its Data Processing Center, and AMSR-E data were provided by NASA Distributed Active Archive Center.

References

[1] Kessler E. On the continuity and distribution of water substance in atmospheric circulations. Atmos Res 1996;2:109–45, http://dx.doi.org/10.1016/0169-8095(94)00090-Z.
[2] Rotstayn LD. On the "tuning" of autoconversion parameterizations in climate models. J Geophys Res-Atmos 2000;D12:5495–15507, http://dx.doi.org/10.1029/2000jd900129.
[3] Suzuki K, Stephens GL. Global identification of warm cloud microphysical processes with combined use of A-Train observations. Geophys Res Lett 2008;8:L08805. http://dx.doi.org/10.1029/2008gl033590.
[4] Suzuki K, Stephens GL, van den Heever SC, Nakajima TY. Diagnosis of the warm rain process in cloud-resolving models using joint cloudSat and MODIS observations. J Atmos Sci 2011;11:2655–70. http://dx.doi.org/10.1175/jas-d-10-05026.1.
[5] Stephens GL, Kummerow CD. The remote sensing of clouds and precipitation from space: a review. J Atmos Sci 2007;11:3742–65. http://dx.doi.org/10.1175/2006jas2375.1.
[6] Khain A, Pinsky M, Magaritz L, Krasnov O, Russchenberg HWJ. Combined observational and model investigations of the Z-LWC relationship in stratocumulus clouds. J Appl Meteorol Clim 2008;2:591–606. http://dx.doi.org/10.1175/2007jamc1701.1.
[7] Matrosov SY, Uttal T, Hazen DA. Evaluation of radar reflectivity-based estimates of water content in stratiform marine clouds. J Appl Meteorol 2004;3:405–19. http://dx.doi.org/10.1175/1520-0450(2004)043<0405:eorreo>2.0.co;2.

[8] Albrecht BA. Aerosols, cloud microphysics, and fractional cloudiness. Science 1989;4923:1227–30. http://dx.doi.org/10.1126/science.245.4923.1227.

[9] Duong HT, Sorooshian A, Feingold G. Investigating potential biases in observed and modeled metrics of aerosol-cloud-precipitation interactions. Atmos Chem Phys 2011;9:4027–37, http://dx.doi.org/10.5194/acp-11-4027-2011.

[10] Guo H, Liu Y, Penner JE. Does the threshold representation associated with the autoconversion process matter? Atmos Chem Phys 2008;5:1225–30. http://dx.doi.org/10.5194/acp-8-1225-2008.

[11] L'Ecuyer TS, Berg W, Haynes J, Lebsock M, Takemura T. Global observations of aerosol impacts on precipitation occurrence in warm maritime clouds. J Geophys Res-Atmos 2009:D09211, http://dx.doi.org/10.1029/2008jd011273.

[12] Wentz FJ. A well-calibrated ocean algorithm for special sensor microwave/imager. J Geophys Res-Ocean 1997;C4:8703–18, http://dx.doi.org/10.1029/96jc01751.

[13] Wentz FJ, Spencer RW. SSM/I rain retrievals within a unified all-weather ocean algorithm. J Atmos Sci 1998;9:1613–27, http://dx.doi.org/10.1175/1520-0469(1998)055 < 1613:Sirrwa > 2.0.Co;2.

[14] Aonashi K, Liu GS. Passive microwave precipitation retrievals using TMI during the Baiu period of 1998. Part I: algorithm description and validation. J Appl Meteorol 2000;12:2024–37, http://dx.doi.org/10.1175/1520-0450(2000)039 < 2024:pmprut > 2.0.co;2.

[15] Berg W, L'Ecuyer T, Kummerow C. Rainfall climate regimes: the relationship of regional TRMM rainfall biases to the environment. J Appl Meteorol Clim 2006;3:434–54. http://dx.doi.org/10.1175/jam2331.1.

[16] Wilheit T, Kummerow CD, Ferraro R. Rainfall algorithms for AMSR-E. IEEE Trans Geosci Remote Sens 2003;2:204–14. http://dx.doi.org/10.1109/tgrs.2002.808312.

[17] Gerber H. Microphysics of marine stratocumulus clouds with two drizzle modes. J Atmos Sci 1996;12:1649–62. http://dx.doi.org/10.1175/1520-0469(1996)053 < 1649:Momscw > 2.0.Co;2.

[18] Masunaga H, Nakajima TY, Nakajima T, Kachi M, Suzuki K. Physical properties of maritime low clouds as retrieved by combined use of Tropical Rainfall Measuring Mission (TRMM) microwave imager and visible/infrared scanner – 2. Climatology of warm clouds and rain. J Geophys Res-Atmos 2002;D19:4367. http://dx.doi.org/10.1029/2001jd001269.

[19] Shao HF, Liu GS. Detecting drizzle in marine warm clouds using combined visible, infrared, and microwave satellite data. J Geophys Res-Atmos 2004;D7:D07205. http://dx.doi.org/10.1029/2003jd004286.

[20] Kawamoto K, Suzuki K. Distributional correspondence of 94-GHz radar reflectivity with the variation in water cloud properties over the northwestern Pacific and China. J Quant Spectrosc Radiat Transf 2015:38–48. http://dx.doi.org/10.1016/j.jqsrt.2014.10.012.

[21] Burnet F, Brenguier JL. The onset of precipitation in warm cumulus clouds: an observational case-study. Q J Royal Meteor Soc 2010;647:374–81. http://dx.doi.org/10.1002/Qj.552.

[22] Wood R, Kubar TL, Hartmann DL. Understanding the importance of microphysics and macrophysics for warm rain in marine low clouds. Part II: Heuristic models of rain formation. J Atmos Sci 2009;10:2973–90. http://dx.doi.org/10.1175/2009jas3072.1.

[23] Leon DC, Wang Z, Liu D. Climatology of drizzle in marine boundary layer clouds based on 1 year of data from CloudSat and Cloud-Aerosol Lidar and Infrared Pathfinder Satellite Observations (CALIPSO). J Geophys Res-Atmos 2008:D00a14. http://dx.doi.org/10.1029/2008jd009835.

[24] Kawamoto K, Suzuki K. Comparison of water cloud microphysics over mid-latitude land and ocean using CloudSat and MODIS observations. J Quant Spectrosc Radiat Transf 2013:13–24. http://dx.doi.org/10.1016/j.jqsrt.2012.12.013.

[25] Haynes JM, L'Ecuyer TS, Stephens GL, Miller SD, Mitrescu C, Wood NB, Tanelli S. Rainfall retrieval over the ocean with spaceborne W-band radar. J Geophys Res-Atmos 2009:D00a22. http://dx.doi.org/10.1029/2008jd009973.

[26] Kubar TL, Hartmann DL, Wood R. Understanding the importance of microphysics and macrophysics for warm rain in marine low clouds. Part I: Satellite observations. J Atmos Sci 2009;10:2953–72. http://dx.doi.org/10.1175/2009jas3071.1.

[27] Lebsock MD, L'Ecuyer TS. The retrieval of warm rain from CloudSat. J Geophys Res-Atmos 2011:D20209. http://dx.doi.org/10.1029/2011jd016076.

[28] Stephens GL, Haynes JM. Near global observations of the warm rain coalescence process. Geophys Res Lett 2007;20:L20805, http://dx.doi.org/10.1029/2007gl030259.

[29] Kogan ZN, Mechem DB, Kogan YL. Assessment of variability in continental low stratiform clouds based on observations of radar reflectivity. J Geophys Res-Atmos 2005;D18:D18205, http://dx.doi.org/10.1029/2005jd006158.

[30] Mace GG, Sassen K. A constrained algorithm for retrieval of stratocumulus cloud properties using solar radiation, microwave radiometer, and millimeter cloud radar data. J Geophys Res-Atmos 2000;D23:29099–108. http://dx.doi.org/10.1029/2000jd900403.

[31] Kato S, Mace GG, Clothiaux EE, Liljegren JC, Austin RT. Doppler cloud radar derived drop size distributions in liquid water stratus clouds. J Atmos Sci 2001;19:2895–911. http://dx.doi.org/10.1175/1520-0469(2001)058 < 2895:dcrdds > 2.0.co;2.

[32] Wang JY, Geerts B. Identifying drizzle within marine stratus with W-band radar reflectivity. Atmos Res 2003;69:1–27, http://dx.doi.org/10.1016/j.atmosres.2003.08.001.

[33] Liu YG, Geerts B, Miller M, Daum P, McGraw R. Threshold radar reflectivity for drizzling clouds. Geophys Res Lett 2008;3:L03807. http://dx.doi.org/10.1029/2007gl031201.

[34] Mace G. Level 2 GEOPROF product process description and interface control document algorithm version 5.3. ⟨http://www.cloudsat.cira.colostate.edu/sites/default/files/products/files/2B-GEOPROF_PDICD.P_R04.20070628.pdf⟩; 2007.

[35] Partain P. Cloudsat ECMWF-AUX auxiliary data process description and interface control document. ⟨http://www.cloudsat.cira.colostate.edu/sites/default/files/products/files/ECMWF-AUX_PDICD.P_R04.20070718.pdf⟩; 2007.

[36] Wang Y, Liu GS, Seo EK, Fu YF. Liquid water in snowing clouds: Implications for satellite remote sensing of snowfall. Atmos Res 2013:60–72. http://dx.doi.org/10.1016/j.atmosres.2012.06.008.

[37] Rogers RR, Yau MKA. Short course in cloud physics. 3rd ed. Woburn, MA: Butterworth-Heinemann; 1989.

[38] Brenguier JL, Pawlowska H, Schuller L, Preusker R, Fischer J, Fouquart Y. Radiative properties of boundary layer clouds: Droplet effective radius versus number concentration. J Atmos Sci 2000;6:803–21. http://dx.doi.org/10.1175/1520-0469(2000)057 < 0803:Rpoblc > 2.0.Co;2.

[39] Martin GM, Johnson DW, Spice A. The measurement and parameterization of effective radius of droplets in warm stratocumulus clouds. J Atmos Sci 1994;13:1823–42. http://dx.doi.org/10.1175/1520-0469(1994)051 < 1823:Tmapoe > 2.0.Co;2.

[40] French JR, Vali G, Kelly RD. Observations of microphysics pertaining to the development of drizzle in warm, shallow cumulus clouds. Q J Royal Meteor Soc 2000;563:415–43. http://dx.doi.org/10.1002/qj.49712656304.

[41] Frisch AS, Fairall CW, Snider JB. Measurement of stratus cloud and drizzle parameters in astex with a K-alpha-band doppler radar and a microwave radiometer. J Atmos Sci 1995;16:2788–99, http://dx.doi.org/10.1175/1520-0469(1995)052 < 2788:Moscad > 2.0.Co;2.

[42] Geoffroy O, Brenguier JL, Sandu I. Relationship between drizzle rate, liquid water path and droplet concentration at the scale of a stratocumulus cloud system. Atmos Chem Phys 2008;16:4641–54. http://dx.doi.org/10.5194/acp-8-4641-2008.

[43] Jensen MP, Vogelmann AM, Collins WD, Zhang GJ, Luke EP. Investigation of regional and seasonal variations in marine boundary layer cloud properties from MODIS observations. J Clim 2008;19:4955–73. http://dx.doi.org/10.1175/2008JCLI1974.1.

[44] Khairoutdinov M, Kogan Y. A new cloud physics parameterization in a large-eddy simulation model of marine stratocumulus. Mon Weather Rev 2000;1:229–43. http://dx.doi.org/10.1175/1520-0493(2000)128 < 0229:Ancppi > 2.0.Co;2.

[45] Wood R. Drizzle in stratiform boundary layer clouds. Part 1: Vertical and horizontal structure. J Atmos Sci 2005;9:3011–33, http://dx.doi.org/10.1175/jas3529.1.

[46] Suzuki K, Nakajima TY, Stephens GL. Particle growth and drop collection efficiency of warm clouds as inferred from joint cloudSat and MODIS observations. J Atmos Sci 2010;9:3019–32, http://dx.doi.org/10.1175/2010jas3463.1.

[47] Bennartz R. Global assessment of marine boundary layer cloud droplet number concentration from satellite. J Geophys Res-Atmos 2007;D2:D02201. http://dx.doi.org/10.1029/2006jd007547.

[48] Wood R. Stratocumulus clouds. Mon Weather Rev 2012;8:2373–423. http://dx.doi.org/10.1175/Mwr-D-11-00121.1.

[49] Chen RY, Li ZQ, Kuligowski RJ, Ferraro R, Weng FZ. A study of warm rain detection using A-Train satellite data. Geophys Res Lett 2011:L04804. http://dx.doi.org/10.1029/2010gl046217.